Numerical Simulation of Remediation of Groundwater Contaminated with Radionuclide and Heavy Metal

Synopsis of the PhD Thesis

Submitted by

Harshita Singh Chauhan

70821017024

Department of Civil Engineering

Supervisor

Dr. Meenal Mategaonkar

submitted in partial fulfilment of the requirements of

DOCTOR OF PHILOSOPHY (Engineering)

MUKESH PATEL SCHOOL OF TECHNOLOGY MANAGEMENT & ENGINEERING

SVKM'sNARSEE MONJEE INSTITUTE OF MANAGEMENT STUDIES (Declared as Deemed-to-be University Under Section 3 of the UGC Act, 1956)

V. L. Mehta Road, Vile Parle (West)

MUMBAI –400056

July 2023

TABLE OF CONTENTS

SECTION NO.	TITLE	PAGE NO.
	ABSTRACT	iii
1	INTRODUCTION	1
2	OBJECTIVES	3
3	LITERATURE REVIEW	3
4	CONTRIBUTION 1: Biosorption of lead II using Foeniculum Vulgare in the aqueous phase	5
	4.1 Experimentation	6
	4.2 Results and analysis	7
	4.3 Adsorption isotherms and models	10
	4.4 Kinetic studies and models	13
	4.5 Experimentation- using real groundwater sample	16
	4.6 Conclusion	17
5	CONTRIBUTION 2: Case Study- MODFLOW/ MT3D groundwater flow and Uranium Transport of Bathinda district, Punjab, India	18
	5.1 Study area	18
	5.2 Groundwater Flow: Conceptual Model	21
	5.3 Sensitivity analysis	27
	5.4 Uranium Transport: Conceptual Model	28
	5.5 Lead Transport: Conceptual Model	30
	5.6 Conclusion	33
6	Future Scope and Limitations	33
7	Publications	34
8	References	35

Abstract

The colossal use of radioactive materials, fossil fuels and mining activities in the medical field, technological development, power generation and industrial sites ha created a great accumulation of radioactive and heavy metal waste. Even a small concentration of this in the environment can have an impact for a longer period. Long term exposure to these leads to an elevated risk of leukemia, leucopenia, kidney damage and genetic damage that can pass into the next generation. Groundwater quality is significantly deteriorated due to radioactive and heavy metal leachate from solid waste landfills, fallouts from nuclear and thermal power plants, etc. Bioremediation techniques are observed to be able to interact with these contaminants and remediate them from the groundwater.

The first part of present study focusses on the experimentation for bioreduction of lead as a contaminant in groundwater. In this study, three biomasses are used which are obtained from Fennel (*Foeniculum vulgare*) plant as Fennel seeds, leaves and stem to treat the synthetic lead contaminated water sample by biosorption. Physicochemical parameters initial concentration of lead, time of contact, biomass quantity and pH of the solution are assessed. Adsorption equilibrium isotherms are modelled using the Langmuir, Freundlich and Temkin models; the Freundlich model provides the best fit for the biosorption process, with a higher correlation coefficient (R^2). This study shows that the Fennel (*Foeniculum vulgare*) powder is an effective adsorbent for the removal of Lead (Pb) from aqueous solution.

The second part of the study focusses on the simulation of ground water flow and transport using MODFLOW/ MT3DMS model. A real-life case study of Akola and Buldhana, Maharashtra, India is performed for simulation of TDS transport in the groundwater of that region for one dimension. Another three-dimensional real-life case study of Bathinda, Punjab, India is performed for simulation of groundwater flow and uranium contaminant transport in the groundwater of that district. The model involved a steady-state hydrogeological simulation of the three-layered aquifer. MODFLOW is proven to be an effective that can be easily implemented to the confined or unconfined aquifers with the consideration of heterogeneity and isotropy.

1. Introduction

Water is essential to life and a nominal supply of clean-safe drinking water is required for the sustenance of life. In developed countries, drinking water quality guidelines and regulations are based on current, published-scientific research related to health effects, aesthetic effects, and operational considerations. In developing countries, it is estimated that over 80% of disease is caused by contaminated drinking water and as a consequence, over 30% of work productivity is lost. Despite a concentrated international effort, significant investment and widespread educational campaigns, access to safe drinking water appears to be in decline.

Water containing trace amounts of various radioactive materials is normally released from nuclear power plants. Radionuclides are also produced during nuclear weapons explosions, and in the fallouts of nuclear reactors producing electricity. Serious contamination of the environment with uranium has been brought up due to wastewater produced by the exploitation and smelting of uranium mines and nuclear power stations along with other industries using uranium radiation material. The mineral materials if drained directly without carrying out appropriate treatment will absorb the poisonous radiation materials, such as uranium. Human health and the ecosystem's safety is endangered when such materials gradually enter into the geochemical circulation and break the organism's normal metabolism. Uranium contaminations can reach the food chain through surface and groundwater and eventually be ingested by humans causing liver damage and even death. Even a small concentration of radionuclide in the environment can have an impact for a prolonged period of time due to their long half-life. Due to the potential toxicity of radioactive contaminants, there is considerable interest in the removal and recovery of it from environmental materials. The WHO states that the amount of uranium per litre of drinking water should not exceed 30 micrograms.

Another major issue in groundwater is the increased concentration of heavy metals as it is particularly harmful because they are persistent, toxic, and non-degradable. All industrial processes generate by-products that become waste materials and have the potential of contaminating the environment. The adverse impact of heavy metals, especially lead, on the environment has been well documented by many researchers [Robert M. Brooks et al. (2010)]. Lead (Pb) is in elemental form, and hence cannot be degraded or transformed into a less dangerous material. Lead even in very low

concentration is very harmful to living organisms. It is observed that the lead exposure in humans can have severe neurological and physiological repercussions.

Impact of lead exposure in humans has been known to cause wide variety of health problems such as: various forms of blood disorders and anaemia, rapid deterioration of brain and the nervous system, reduced fertility both in men and women, failure of the kidney, Alzheimer disease etc.

***Causes of Radionuclide & Heavy Metal Contamination*:**

• Biomedical radioactive waste

• Industrial sites

• Nuclear power plants

• Uranium mining

• The leaching of contaminants deposited by fallout

• Nuclear weapons program

• Waste incineration

• Commercial fuel reprocessing

• Electronic waste

• Nuclear accidents

Biosorption

Biosorption is a physiochemical process that occurs naturally in certain biomass, which allows it to passively concentrate and bind contaminants onto its cellular structure. It is an alternative method, which utilizes all kinds of biological natural materials, such as bacteria, fungi, yeast, algae. The advantages of this method compared with the traditional method are metal sequestering properties, decreasing the soluble concentration of heavy-metal ions, simple operation, abundant sources of biosorbents, fast adsorbing speed and high efficiency and selectivity for adsorbing heavy metals in low concentrations, energy saving, broad operational range of pH and temperature, easy reclamation of heavy metal, and easy recycling of the biosorbents, etc. It is a scientific and practical solution to develop low-cost and easily available uranium sorbents to improve the liquid–solid separation during the process and enhance the efficient treatment of uranium-containing wastewater.

2. Objective of this research

This research work is divided into two parts:
Contribution 1- Biosorption of lead II using Foeniculum Vulgare in Aqueous Phase:

- Biosorption is examined by the use of three biomasses obtained from foeniculum vulgare (fennel) plant i.e., its seeds, leaves and stem to treat the lead (II) contaminated water.
- This study focuses on the use of fennel seeds, leaves and stem as a biosorbent to remediate lead contaminated water. Several experiments are conducted to find at the feasibility of this biosorbent for bioremediating lead contaminated water.
- The objective is to prove that this basic treatment is feasible in even small villages where proper facilities are not available.

Contribution 2- Numerical Simulation for three-dimensional groundwater flow and transport of Uranium contaminant in Bathinda district, Punjab, India:

- The objective of this study is to calibrate and validate the MODFLOW and MT3D model for the groundwater flow and uranium transport in the study area and then to predict the future scenario for the year 2030 to forewarn the risks involved with it.
- The groundwater is the primary source of drinking water in the study area and the predicted uranium concentration found in this study will act as a warning alarm to start with the preventive measures to avoid major health hazard of the inhabitants in the times to come.

3. Literature Review

Liangshu Xia et al. (2013) used banyan leaves (BLs) for biosorption of uranium ions from wastewater. The adsorption behavior, thermodynamics, and kinetics of this biosorption process were studied. The results showed that the optimal adsorption was achieved at pH 3.0, initial metal concentration100 ppm and biosorbent dosage 5 g/L. The biosorption process of Uranium ions achieved equilibrium at 50 min contact period. This research concluded that banyan leaves prove to be acceptable biosorbent for removal of Uranium from wastewater.

The ability of live and dead biomass of indigenous Aspergillus Niger was examined **by Sana Solat (2014)** for the removal of uranium (VI) from dilute aqueous solutions. The

influences of different experimental parameters such as initial solution pH, initial uranium concentration, biomass concentration, and contact time were investigated. The results indicated that the maximum sorption of biomass was observed at pH 5 and pH 4, and biosorption equilibrium was established in 120 and 60 min, for live and dead biomass, respectively. Optimal biosorption was observed at concentrations of 0.2 and 0.3 g dry biomass per 100 mL for live and dead biomass, respectively.

Alkali Ash Material Permeable Reactive Barrier (AAM-PRB) made with fly ash alkali activating solution and filler material was used by **Robert Brooks et al. (2010)** to remove lead (Pb) from contaminated water. AAM-PRB materials with high permeability were created. AAM - PRB from three ash sources with permeability of 10-1 cm/sec were produced and crushed into pellets. Effectiveness of the various barriers was determined by batch and column tests. Laboratory experiments indicate lead ion reduces from 1000 ppm to less than 2 ppm with 10 liters of solution and Lead ion from 10 ppm to less than 0.01 ppm. Analyses were performed by atomic adsorption techniques.

B.S. Bajwa et. Al. (2017) used Laser Fluorimetry technique for the microanalysis of uranium content in drinking water samples collected from different sources like the hand pumps, tube wells of various depths from wide range of locations in the four districts of SW-**Punjab, India**. The purpose of this study was to investigate the uranium concentration levels of ground water being used for drinking purposes and to determine its health effects, if any, to the local population of this region. Corresponding radiological and chemical risks have also been calculated for the uranium concentrations in ground water samples. Some other heavy elements have also been analyzed using the Atomic Absorption Spectrometry. In this region, uranium concentration in 498 drinking water samples has been found to vary between 0.5–579 $\mu g l^{-1}$with an average of 73.5 $\mu g l^{-1}$. Data analysis revealed that 338 of 498 samples had uranium concentration higher than recommended safe limit of 30 $\mu g l^{-1}$ while 216 samples exceeded the threshold of 60 $\mu g l^{-1}$ recommended by AERB, DAE, India, 2004.

Sushant Kumar et. al., 2017 focused on groundwater recourse assessment through steady-state flow modelling in Bina River basin. Bina River is a tributary of Betwa River and is the main source of water for domestic water supply and irrigation supply. Despite its importance for the people in the region, the hydrogeological system of the

Bina River basin is not well understood. The model involved a steady-state hydrogeological simulation of the two-layered aquifer. The groundwater modelling approach was found to be efficient in identifying the dominant hydrological processes in Bina River basin including evapotranspiration and recharge. The model domain was delineated based on field traverses, topographic maps and digital elevation model extracted from Survey of India toposheet contour lines in ILWIS platform. Aquifer parameters were assigned based on given data by CGWB and WRD, which were then adjusted during the model calibration. The main recharge mechanism considered was direct recharge from rainfall. The model was calibrated to static water levels during 2009 pre- monsoon in each block of Bina River Basin. The overall model results are comparable with the observation well data. The sensitivity of the calibrated model was tested by systematically changing one parameter or input variable at a time and it was found that the model is highly sensitive to changes in ET and recharge rate.

4. Contribution 1: Biosorption of lead II using Foeniculum Vulgare in the aqueous phase

All the experimental work in current study is carried out in environmental engineering laboratory at NMIMS's Mukesh Patel School of Engineering, Mumbai. Proper care is taken while taking the samples to the lab to maintain the chemical properties of the prepared samples. The safety of those involved in the experiments is assured by the means of facemasks and rubber gloves to avoid any harmful effect of lead. Pure and analytical grade chemicals are used in all experiments including media preparation for Biosorption. All the biosorbents are procured from authorized stores and were of best grade. The initial tests for standardization of the experimental set up is done with banyan and mango leaves as biosorbents. The results are then verified with the literature and then foeniculum vulgare was used as the biosorbent for the study.

Foeniculum vulgare (fennel) plant is a perennial herb abundantly grown in India, used as an ingredient in Indian spices and medicines. It is used in different forms for dental health, problems related to intestines, digestive disorders and is eaten raw to improve eyesight. Due to its medicinal properties and accessibility in India, it would be a good choice as a biosorbent, also, drinking water treated with fennel would not be fetid or unpleasant to taste.

This study focuses on the use of fennel seeds, leaves and stem as a biosorbent to remediate lead contaminated water. Several experiments are conducted to find at the feasibility of this biosorbent for bioremediating lead contaminated water.

Preparation of biosorbent

In the actual study, three biomasses are used obtained from fennel (*foeniculum vulgare*) plant, i.e., fennel leaves, fennel seeds and fennel stem. These are washed thoroughly with double distilled water (DDW) to get rid of water-soluble impurities and surface adhered particles. The biomasses are then sundried for about 72-96 hours to remove all the moisture trapped inside the particles. They are then crushed and sieved to a fragment size of 100-300μm and were stored in an airtight container to avoid any further contact with moisture.

Preparation of Synthetic Lead sample

A stock solution of lead is prepared by dissolving powdered form of lead nitrate [$Pb(NO_3)_2$] in distilled water. Further dilution of this solution is done to obtain the required metal ion concentrations. The pH of solutions is adjusted with 0.1N HCl and NaOH. All chemicals were of AR grade. Atomic Absorption Spectrometer (AAS) is used to determine the lead concentration in the prepared solution. (Surisetty et al., 2013)

$$2Pb(NO_3)_{2(s)} + 2H_2O_{(l)} = 2Pb(s) + O_{2(g)} + 4HNO_{3(l)}$$

$$2HNO_{3\,(l)} + 2HCl_{(l)} = 2NO_{2(g)} + 2H_2O_{(l)} + Cl_{2(g)}$$

4.1 **Experimentation**

Samples of 30ml each of different lead concentrations are taken for batch experiments at room temperature (27 $\pm$ 1° C). The different quantities of biomass are added in each of the beaker. It is then placed on the magnetic stirrer rotating at a speed of 180 rpm for different contact times for each of the sample. (Surisetty et al., 2013)

After the biosorption process, the biosorbent is filtered from the solution with the help of whatman-42 filter paper. To determine the optimum quantity of biomass, the filtered sample is tested under Atomic Absorption Spectrophotometer (AAS) for metal concentration detection. All experiments are performed in three sets and outcomes are reported as mean. The biosorption capacity at the time of equilibrium q_e (mg/g) is given as (Amin et al., 2015):

$$q_e(mg/g) = (C_o - C_e)\text{x}\,\frac{V}{m} \qquad (1)$$

where C_o [M L^{-1}] is the liquid-phase concentration of solutes at the initial stage and C_e [M L^{-1}] is equilibrium lead concentration, V is the sample volume taken for tests [L^3] and *m* is mass of the biosorbent [M].

Figure 1: Fennel Biomass dried under direct sunlight

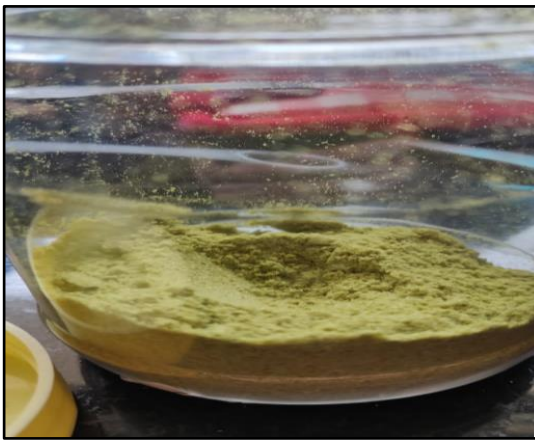

Figure 2: Fennel Seed in powdered form- Biosorbent

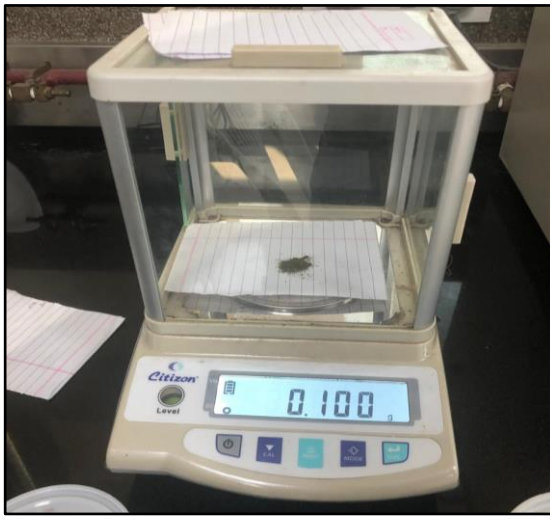

Figure 3: Weighing biomass quantity needed for biosorption

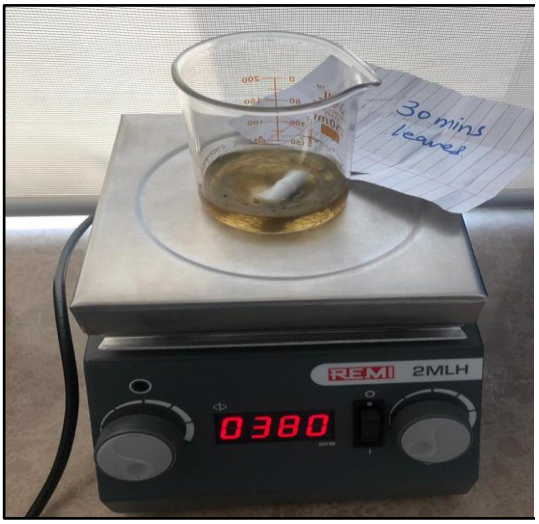

Figure 4: Sample under biosorption using a magnetic stirrer

4.2 Results and analysis

Effect of initial concentration of lead ion

An increase in the metal ion concentration led to decrease in the percentage adsorption. Different lead concentrations are taken viz. 1, 5, 10, 15 and 20ppm for a contact time of 45min and biomass concentration of 0.1 grams (as per the preliminary biosorption testing). The plot of reduction in adsorption efficiency with increase initial concentration of lead in the solution for the three biomasses is shown in Figure 5. Dearth of binding sites and insufficient surface area of biomasses can be the reasons of

reduction in percentage adsorption (Surisetty et al., 2013). As the concentration of metal ions increases, its interaction with the binding sites reduces and thus the percentage of adsorption was lower at higher lead ion concentrations.

Optimization of contact time

For the optimum contact time, different quantities of all the three biomasses viz. 0.01, 0.05, 0.10, 0.15, 0.20 and 0.030 grams are added to the sample with different contact times viz. 5, 10, 15, 30, 45, and 60mins. The optimum contact time of 45min is observed to achieve equilibrium, and there was no change in the adsorption efficiency beyond that. The contact time of further experiments is taken as 45 min. The plot of graph in Figure 6 shows that the maximum adsorption efficiency of 70%, 80% and 77% for fennel seeds, leaves and stem respectively is achieved in the first 45min, and at this stage equilibrium is attained. The availability of the large surface area in the first part of the process is found to be the cause of this behaviour.

Effect of biosorbent dosage

The different quantities of powdered biomass viz. 0.01, 0.05, 0.10, 0.15, 0.20 and 0.30 grams of foeniculum vulgare seeds, leaves and stem are added in different beakers and the experimentation is conducted for a contact time of 45 minutes for each of the sample. The initial concentration of lead in the water sample is taken as 1 ppm. With the addition of biomasses, it got reduced to a mean minimum value of 0.3, 0.2 and 0.23 ppm by multiple tests performed with foeniculum vulgare seeds, leaves and stem respectively. The mean optimum quantity of biosorbent for bioremediation came out to be 0.1g for all the three biomasses. The results are compiled in Figure 7. Metal uptake was very fast in the beginning and slowed down gradually indicating penetration into the interior of the adsorbent particles.

Effect of pH of water sample

The metal uptake is found to be directly proportional to pH from values of 2.0 to 6.4 and gradual decrease was observed at pH 7. The plot of adsorption efficiency with pH values is shown in Figure 8. Analogous observations are made with various biosorbents (Surisetty et al., 2013). The increase in lead adsorption with rising values of pH from 2.0 to 6.4 can be due to the gradual reduction in the clash between proton and metal ion for surface sites. As the value of pH rises, the exposure of ligands in fennel biosorbent causes increase in its negative charge density, which leads to increase in the attraction of positively changed lead ions thus allowing higher adsorption. Thus, the pH value for further biosorption experiments is taken as 6.4.

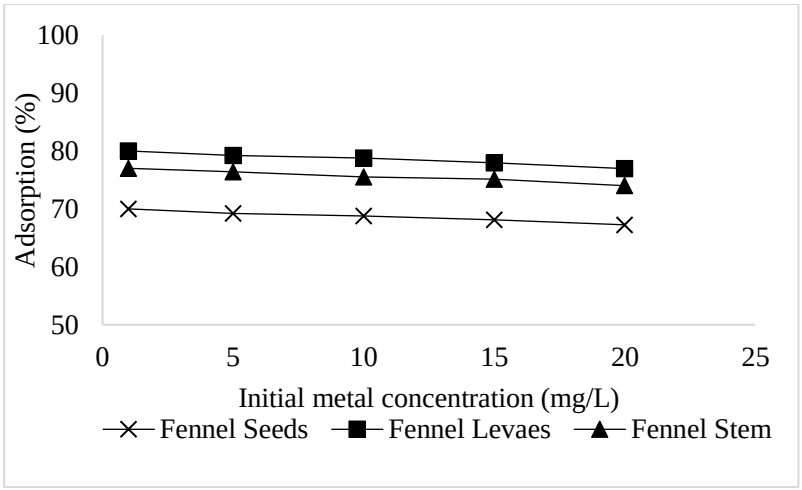

Figure 5: Effect of initial concentration of lead on adsorption efficiency (biosorbent dosage = 0.1 g/30mL, pH = 6.4, t = 45min)

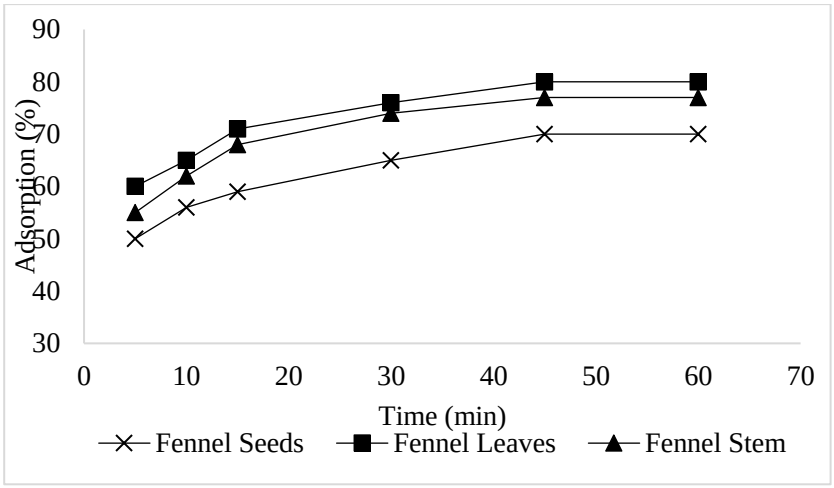

Figure 6: Effect of contact time on lead adsorption efficiency (biosorbent dosage = 0.1 g/30mL, Co = 1mg/L, pH = 6.4)

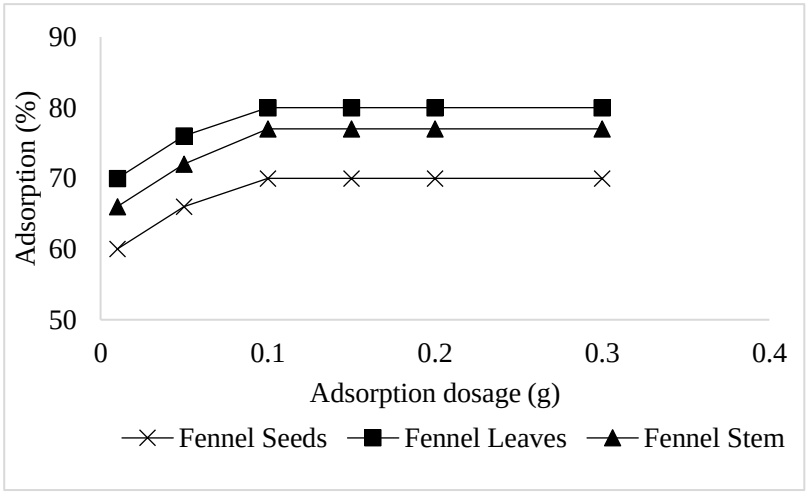

Figure 7: Effect of biosorbent dosage on lead adsorption efficiency (Co = 1mg/L, pH = 6.4, t = 45min

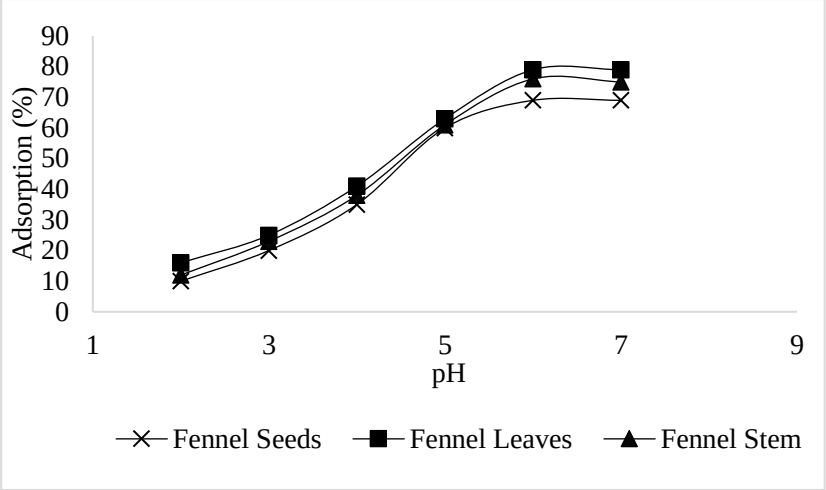

Figure 8: Effect of pH on lead adsorption efficiency (biosorbent dosage = 0.1 g/30mL, Co = 1mg/L, t = 45min

4.3 Adsorption isotherms and models

Adsorption isotherms signals the distribution of molecules subjected to adsorption at equilibrium time between liquid and solid phases. They give an idea about the adsorption mechanism along with the surface properties and affinities of the adsorbent. One of the most important aspects in analysing the mechanism of the adsorption are the equilibrium adsorption isotherms. The results obtained are analysed using Langmuir, Freundlich and Temkin adsorption isotherm models.

Langmuir adsorption isotherm

The assumption of langmuir adsorption isotherm model is that adsorption takes place within the adsorbent at specific homogeneous sites. The Langmuir isotherm model in its linear form (Amin, 2018; Piccin et al. 2011, Ghogomu et al. 2013) is:

$$\frac{C_e}{q_e} = \frac{C_e}{q_m} + \frac{1}{K_L q_m} \qquad (2)$$

where q_e (mg g^{-1}) is the adsorption capacity at equilibrium; C_e (mg L^{-1}) is concentration of lead at equilibrium; K_L is the Langmuir constant (L mg^{-1}) related to the free energy of adsorption and q_m is the monolayer adsorption capacity of the adsorbent (mg g^{-1}). A plot of C_e /q_e versus C_e gives a straight line of slope 1/q_m and intercept 1/ (K_L* q_m). These parameters are calculated with the help of graph in Figure 9.

Freundlich Adsorption Isotherm

The Freundlich adsorption model's linear equation is (Amin et al., 2015; Piccin et al.2011, Ghogomu et al.2013)

$$lnq_e = lnK_F + \frac{1}{n}\, lnC_e \qquad (3)$$

Where, K_F (mg g-1) and n (dimensionless) are the Freundlich adsorption isotherm constants, shows the extent of the adsorption and the degree of nonlinearity, respectively. Graphs for lnCe versus lnqe is plotted to find the intercept value of K_F and the slope value of n, respectively, as shown in Figure 10.

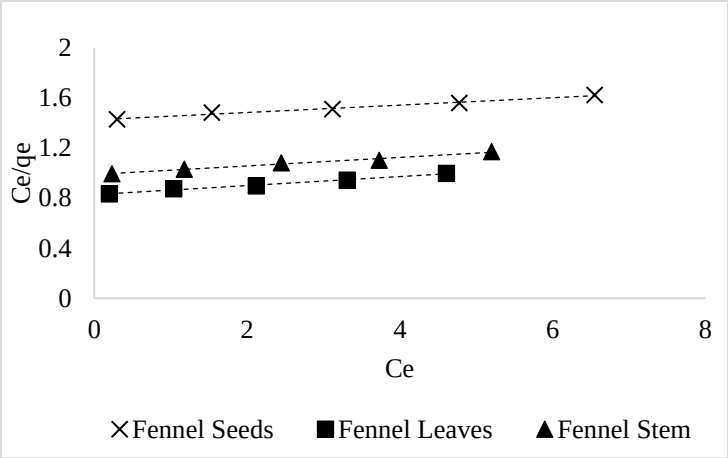

Figure 9: Langmuir adsorption isotherm plot for biosorption of lead (biosorbent dosage = 0.1 g/30mL, pH = 6.4, t = 45min)

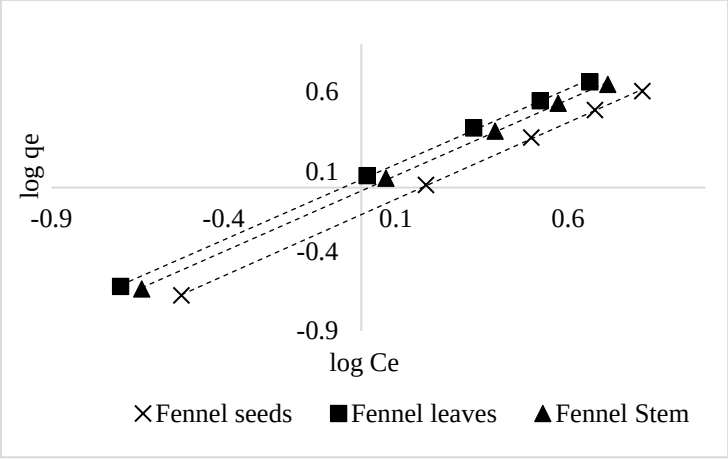

Figure 10: Freundlich adsorption isotherm plot for biosorption of lead (biosorbent dosage = 0.1 g/30mL, pH = 6.4, t = 45min)

Temkin Adsorption Isotherm

This model considers the effects of indirect interactions of the adsorbate on the adsorption process (M. Temkin, 1940) it is assumed that with increase in surface coverage the heat of adsorption ΔHads of all molecules in the layer decreases linearly (Ringot et al. 2007). The linear form of Temkin isotherm model is (Shahbeig et al. 2013):

$$q_e = \frac{RT}{b} lnK_T + \frac{RT}{b} lnC_e \quad (4)$$

Where, K_T is the equilibrium binding constant (L mol^{-1}) corresponding to the maximum binding energy, b is related to the adsorption heat, R is universal gas constant (8.31 J/mol. k), T is absolute temperature and B = RT/b, is the another constant related to the heat of adsorption (Amin et al., 2015; Piccin et al. 2011, Ghogomu et al. 2013). These constants are calculated from the plot q_e vs. ln C_e as shown in Figure 11.

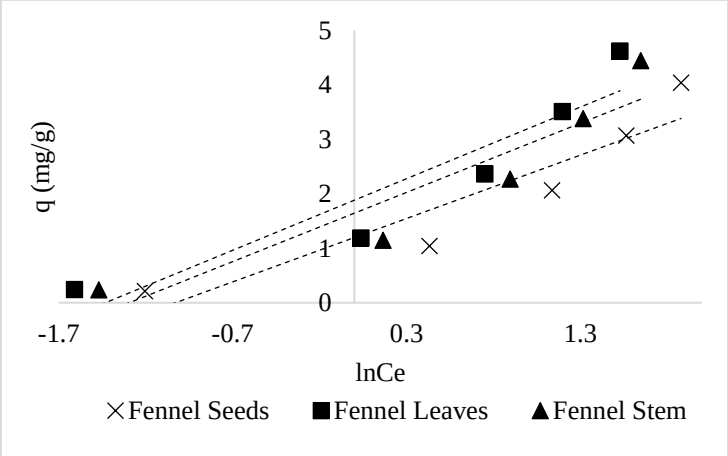

Figure 11: Temkin adsorption Isotherm plot for biosorption of lead (biosorbent dosage = 0.1 g/30mL, pH = 6.4, t = 45min)

Table 1: Langmuir, Freundlich, Temkin adsorption isotherm parameters

Langmuir isotherm constants	Foeniculum Vulgare Seeds	Foeniculum Vulgare Leaves	Foeniculum Vulgare Stem
q_m (mg g^{-1})	33.898	27.770	29.411
K_L (L mg^{-1})	0.020	0.043	0.034
R^2	0.9861	0.9882	0.9850
Freundlich isotherm constants			
K_f (mg g^{-1})	0.8440	1.0517	0.9794
n	1.0383	1.0543	1.0492
R^2	**0.9998**	**0.9995**	**0.9996**
Temkin isotherm constants			
K_T (L mol^{-1})	2.9132	4.1859	3.6475
B	2228.62	1896.54	1963.30
R^2	0.8673	0.8724	0.8705

4.4 Kinetic studies and models

The relationship of biosorption time and solute uptake rate is described by adsorption kinetics. With the aim of analysing the adsorption kinetics in different kinetic models, the pseudo-first-order and second-order models are applied to the sorption data.

Pseudo-First-Order Model

The equation for pseudo-first order kinetics initially introduced by Lagergren (Lagergren, 1898) assumes that adsorption rate and the number of unoccupied sites are directly proportional.

$$\frac{dq_t}{dt} = k_1(q_e - q_t) \tag{5}$$

Where q_t (mg g^{-1}) is the amount of adsorbed lead ions per unit weight of biosorbent at time t and q_e (mg g^{-1}) is the amount of adsorbed lead ions per unit weight of biosorbent at equilibrium time; k_1 (min^{-1}) is the rate constant of pseudo-first order kinetics.

The following equation is obtained after application of the boundary conditions, i.e. at $t = 0$, $q_t = 0$ and at $t = t$, $q_t = q_t$. After integrating Eq. (4), we get,

$$\ln(q_e - q_t) = lnq_e - k_1 t \tag{6}$$

The values of q_e and rate constant are determined from the intercept and the slope of linear plots of $ln\,(q_e - q_t)$ versus t.

Pseudo-Second-Order Model

The formula for pseudo-second order kinetics is as follows:

$$\frac{dq_t}{dt} = k_2(q_e - q_t)^2 \tag{7}$$

where k_2 (g mg^{-1} min^{-1}) is the pseudo second-order rate constant. The integration of this equation from $t = 0$ to $t = t$ and $q_t = 0$ to $q_t = q_t$, leads to the formation of linearized form as follows (Hosseini et al., 2010):

$$\frac{t}{q_t} = \frac{1}{k_2 q_e^2} + \frac{t}{q_e} \tag{8}$$

The intercept and slope of plot of t/q_t versus t, gives the values of the parameters k_2 and q_e. The values of coefficient of determination and the similarity in experimental and calculated q_e values are the two indicators to decide whether the system follows pseudo-first-order or pseudo-second-order kinetic models. The graphs for pseudo-first-order and pseudo-second-order kinetic models are shown in Figure 12 and 13 and their constants for different biomasses are given in Table 2.

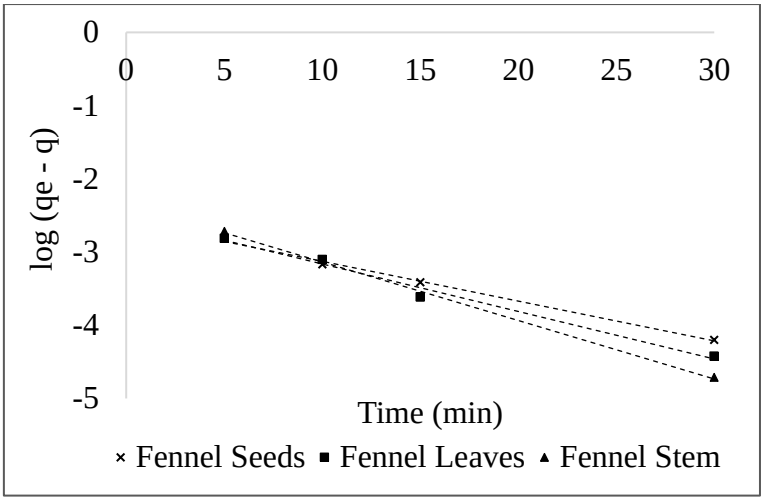

Figure 12: Pseudo-first-order kinetic plot for biosorption of lead

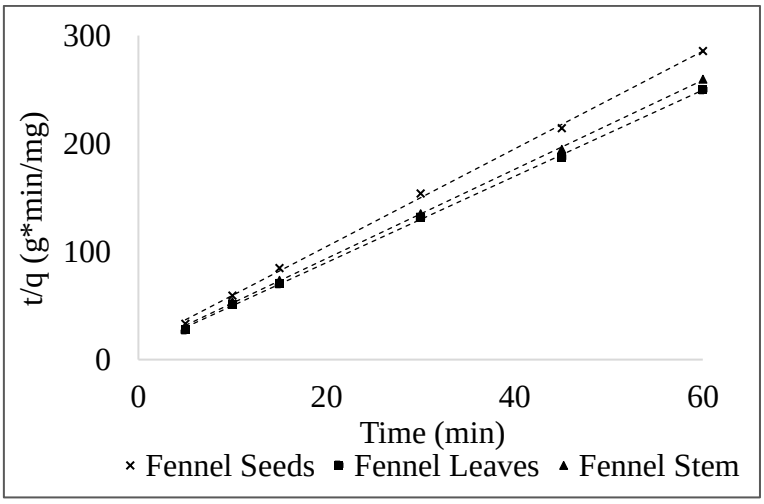

Figure 13: Pseudo-second-order kinetic plot for biosorption of lead

The initial biosorption rate (h) is calculated from the second-order rate constant by the following equation:

$$h = k_2 q_e^2 \tag{9}$$

where h is the initial biosorption rate (mg g^{-1} min^{-1}); q_e is the amount of adsorbed lead ions per unit weight of biosorbent at equilibrium (mg g^{-1}), and k_2 is the equilibrium rate constant of the pseudo–second-order model (g mg^{-1} min^{-1}) (Sahoo et al., 2020). The initial rate of biosorption comes out to be 0.07, 0.10 and 0.09 mg/g min for fennel seeds, leaves and stem respectively. This model concedes that the initial biosorption rates (h) is directly proportional to the initial metal ion concentration. The probability of collisions between these species decreases with decrease in the concentration of lead ions in the solution. Another assumption of this model is the two stage of reaction rates. The first stage claims a higher reaction rate and reaches equilibrium in lesser time after which the second stage with a lower reaction rate continues for an elongated period.

Table 2: Pseudo first and second order kinetics model constants

Kinetic parameters	Foeniculum Vulgare Seeds	Foeniculum Vulgare Leaves	Foeniculum Vulgare Stem
Pseudo-first-order kinetics			
q_e (mg g^{-1})	0.0754	0.0809	0.0966
k_1 (min^{-1})	0.0543	0.0649	0.0799
R^2	0.9962	0.9857	0.9965
Pseudo-second order kinetics			
q_e (mg g^{-1})	0.2211	0.2504	0.2423
k_2 (g mg^{-1} min^{-1})	1.4375	1.6002	1.5406
R^2	0.9990	0.9996	0.9998
Experimental value q_e (mg g^{-1})	0.21	0.24	0.231
Error %	5.02%	4.15%	4.66%

To obtain the instantaneous rate of reaction for the reduction of metal ion in the solution, a simple graph between Ct and t is plotted where Ct [mg/L] is the liquid-phase concentration of solutes with respect to time. The tangent at any point in this graph will give the instantaneous rate of the reaction at that time. The maximum rate was achieved in the beginning of the reaction i.e., the first 5 minutes of the biosorption process as seen in Fig 14 where the metal concentration in the solution dropped to around 50% of its initial value.

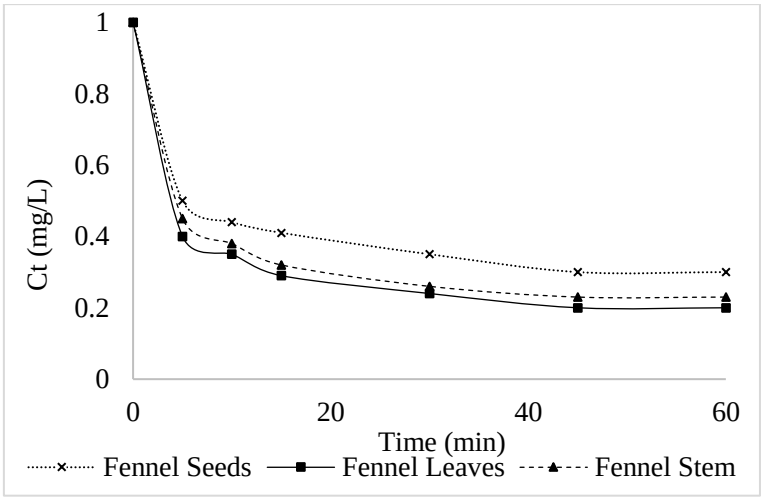

Figure 14: Ct vs t plot for biosorption of lead (biosorbent dosage = 0.1 g/30mL, Co = 1mg/L, pH = 6.4, t = 45min)

Among the three biomasses, fennel leaves gave the best results in terms of efficiency followed by fennel stem and then fennel seeds. The difference in the behaviour of biomasses can be due to their different functional groups like carboxylic or phenolics contained by the cellulosic material in their cell wall as biosorption is a result of cation exchange between metal ion and the functional group.

Gibbs free energy

The spontaneity of the adsorption process between metals and the biomass is expressed by the negative values of Gibbs free energy. The Gibbs free energy of the biosorption process was calculated using equation described by (Ebelegi et al., 2020):

$$Kc = \frac{Ca}{Ce} \tag{10}$$

$$\Delta Go = -RTlnKc \tag{11}$$

Where, ΔG^o is change of gibbs free energy ($J.mol^{-1}$) R is gas constant (8.314 $J\ mol^{-1}\ K^{-1}$), T is temperature (K), K_c is the equilibrium constant, Ca is the amount of biosorbate adsorbed at equilibrium ($mg\ L^{-1}$) and Ce is the equilibrium concentration of biosorbate in solution ($mg\ L^{-1}$) (Ebelegi et al., 2020).

The average values of ΔG^o are calculated to be -1.958 $KJ\ mol^{-1}$, -3.224 $KJ\ mol^{-1}$ and -2.608 $KJ\ mol^{-1}$ respectively for fennel seeds, leaves and stem.

4.5 Experimentation- using real groundwater sample

After successful experimentation of biosorption of synthetic lead sample, a study was done using a real groundwater sample from Devas (76.05, 22.95). The initial lead concentration of the sample was 0.73 mg/l, pH was 7.65, biosorbent dosage used was 0.1 g/30mL and contact time was 45min. Figure 15 and 16 shows the results of this experiment. The results shows that the efficiency of fennel leaves was highest followed by fennel stem and then fennel seeds. The adsorption efficiency for the real sample was less than the synthetic sample due to interference of other contaminants which are also adsorbed in the biosorbent.

Disposal of contaminated biomass

Proper disposal of heavy metal-contaminated biomass can be done by three methods, namely, incineration, composting, and pyrolysis. Among these methods a problem of secondary pollution emerges in incineration and composting and heavy metals will be dispersed into environment. Pyrolysis on the contrary functions in a closed chamber,

thus controlling the dispersion of heavy metals. Hence, pyrolysis is recommended for post-treatment of heavy metal-contaminated biomass (Liu et al., 2003).

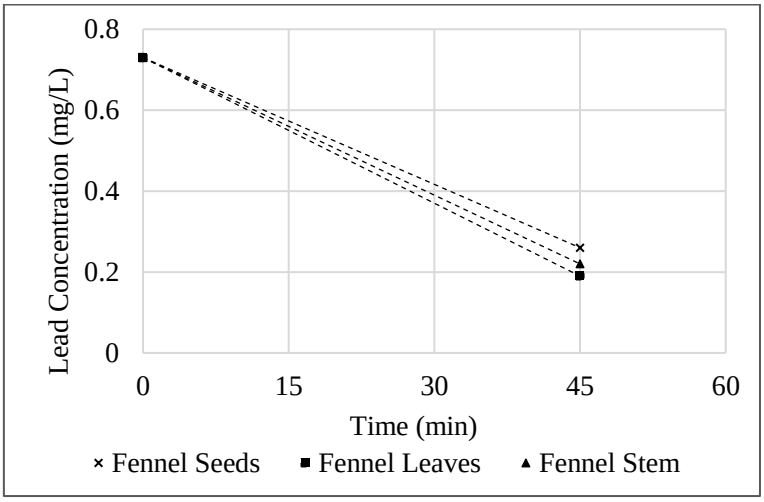

Figure 15: Lead concentration vs time graph for fennel biomass (biosorbent dosage = 0.1 g/30mL, pH = 7.65, t = 45min)

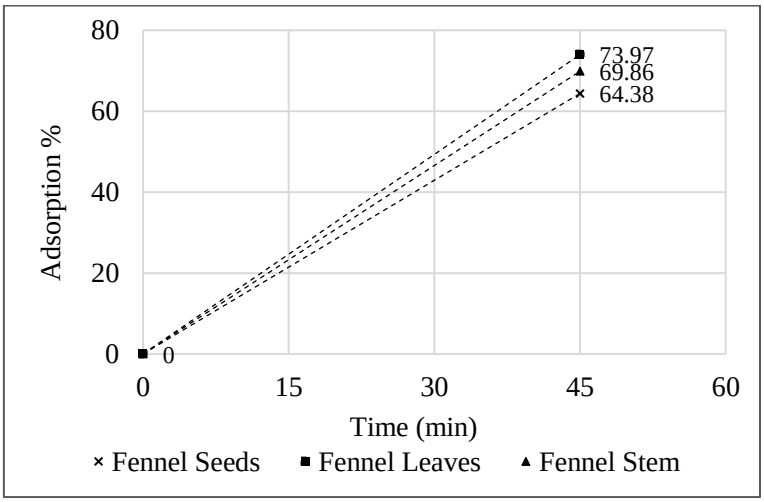

Figure 16: Lead removal efficiency vs time graph for fennel biomass (biosorbent dosage = 0.1 g/30mL, pH = 7.65, t = 45min)

4.6 Conclusion

The above study shows that the powdered form of fennel seeds, leaves and stem is a moderately effective, feasible and economical adsorbent for the removal of lead [Pb(II)] from drinking water. The biosorption efficiency for fennel leaves powder is found to be the highest within same contact time followed by fennel stem and then fennel seeds powder. The experimental results follow pseudo-second-order kinetic model. The process is exothermic as indicated with a negative gibbs free energy value. There are other biosorbents such as banyan leaves, mango leaves etc. which provides better

efficiency but fennel being herb with medicinal properties and sweetening taste, can be a good choice for biosorption of drinking water.

5. Contribution 2: Case Study- MODFLOW/ MT3D groundwater flow and Uranium and Lead Transport of Bathinda district, Punjab, India

5.1 Study area

Bathinda district is in the southern part of Punjab State in the heart of Malwa Region. The area lies between 29°33' to 30°36' North latitude and 74°38' to 75°46' East longitude and falls in Survey of India Toposheet nos. 44J, K, N, and O, covering a geographical area of 3547 sq km. Figure 17 shows the location map of the study area. Total Population of the district, as per the 2011 Census, is 13, 88,525. The population density is 414 persons/ sq.km and the population growth is 17.34 % (CGWB, 2017).

Rainfall: The climate of Bathinda district is classified as tropical, semi-arid and hot which is mainly dry except in rainy months and characterised by intensely hot summer and cold winter. The Average Annual Rainfall is 381.32 mm, which is unevenly distributed over the district. The southwest monsoon sets in last week of June and withdrawn towards end of September and contributes about 82% of annual rainfall. July and August are the wettest months. The remaining of 18% of the annual rainfall occurs during non-monsoon months of the year in the form of thunderstorm and western disturbances.

Land use Land cover: The different classes of LULC Map in Figure 18 along with the area and its percentage was calculated and represented in table 3.

Table 3: Area Distribution within the District as per LULC

Category	Area (in ha)	Area (in %)
Settlements	34408.15	10.24
Agriculture	297238.80	88.46
Waterbodies	429.20	0.13
Open Scrubs/ Waste Land/ Stone Waste	1683.77	0.50
Dense Trees	2103.77	0.63
Bare grounds	144.96	0.04
Total	336008.64	100.00

The main classes are Built Up land, Agricultural land, forestland, Land under non agriculture use, current fallows, and water body. As per the LULC Map, the entire study area comprises of agricultural land which is 297238.80 ha i.e., 88.46% of the total geographical area. The Maximum human settlement's lies in the central region of Bathinda district.

***Digital Elevation Model & Geomorphology along with soil type*:** The Bathinda district lies in the long stretch of Indo-Gangetic plains that is entirely composed of alluvium. There are no surface features like hills, plateau or Isenberg structures. The maximum elevation of the area is 244 m. amsl. and the minimum elevation is 179 m. amsl, as deliberated through SRTM data from USGS. The DEM of the district is shown in Figure 19. The General slope of the study area is found to be towards Southwest direction. Geomorphologically the area is comprising with older alluvium along with aeolian plain, aeolian dune complex. The arid brown soils are found in mostly eastern parts of the district and siezoram soils are found in the western part of the district. Figure 20 shows the geomorphological map of Bathinda District.

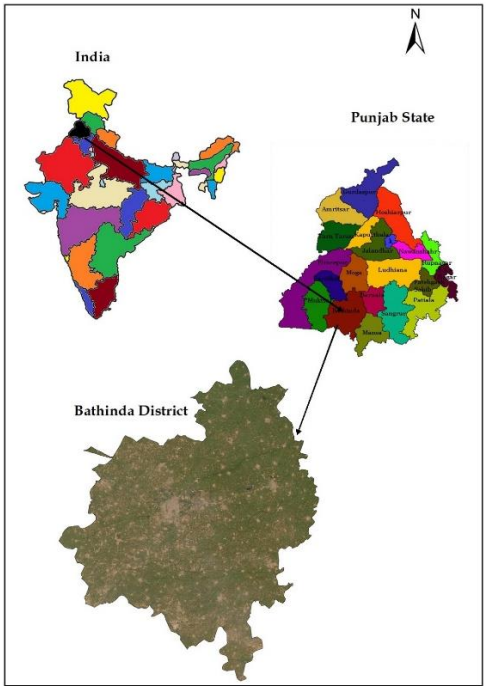

Figure 17: Location map of Study area (Bathinda District)

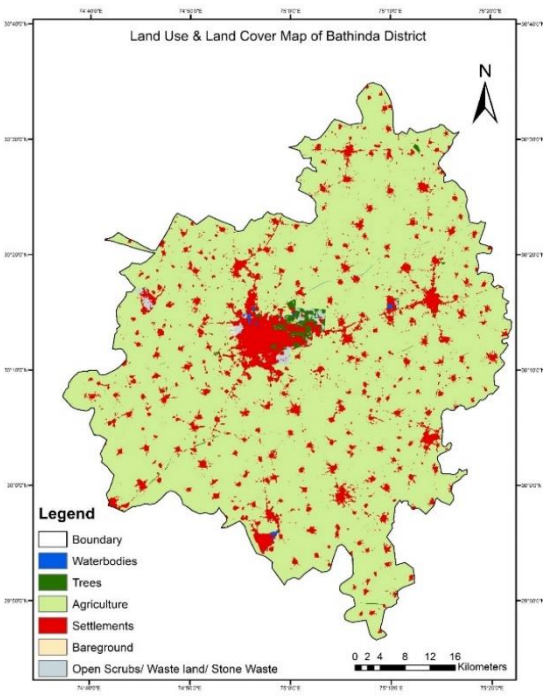

Figure 18: LULC map of Bathinda District (source: ESRI Living Atlas)

***Geology of the Study area*:** Geologically, the area is occupied by a thick sequence of Quaternary deposits of Mid- Pleistocene to Recent age. These comprise alternate

sequence of fluvial and arid phases (Singh, 1993). In this area, water-bearing formations mainly include fine to medium grained sand Kankar with admixture of little clay. The Ground water occurs in unconfined (water table) and confined conditions.

The principal Aquifer in the study area is Alluvium and the Major Aquifers are Older Alluvium and Aeolian Alluvium (CGWB 2017). Figure 21 shows the geological map of Bathinda District, according to which the alluvium is overlain by windblown/sand in various places the wind-blown sand is composed mainly of fine-grained quartz-sand with admixture of muscovite.

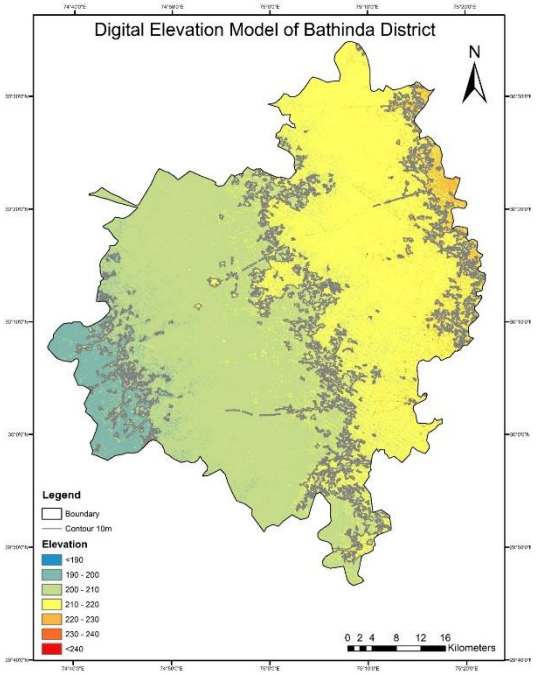

Figure 19: Elevation Map of Bathinda District (Source: USGS earth explorer _SRTM data)

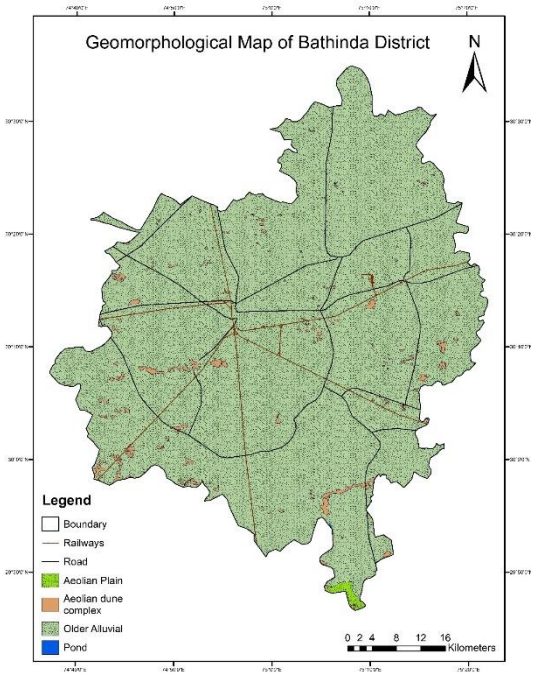

Figure 20: Geomorphological map of Bathinda District

Hydrology and Drainage: No river is flowing through the area, but there are some drains which flow during heavy rains and serve as natural drainage. The main drains are Chand Bhan Drain and Bassian out fall Drain (Figure 22). The main canals are Bathinda branch, Ghaggar branch and the Kotla branch of the Sirhind canal. The Bhakhra main canal runs along the southern part of the area. All the canals are unlined, except for Bhakhra main canal which is lined.

The ground water level in the study area/ Bathinda region varies between 3.26 m below ground level to 33.21 m below ground level. The highest ground water level in mbgl is towards the north east region while the lowest ground water level in mbgl is towards the South west direction.

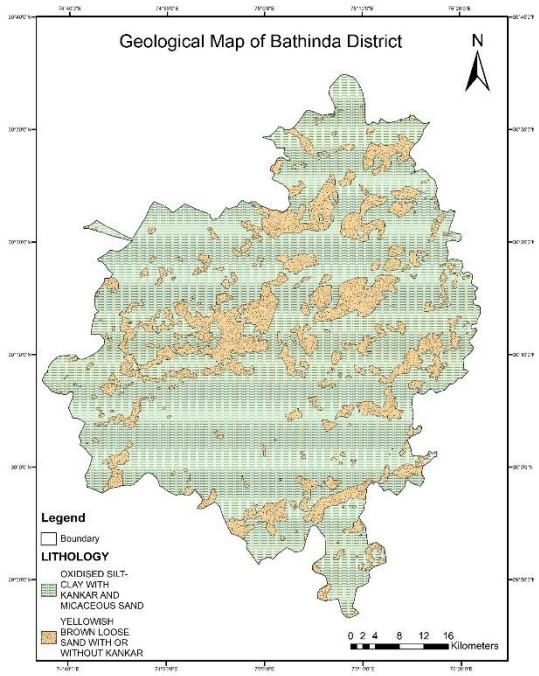

Figure 21: Geological map of Bathinda District (Source Bhukosh)

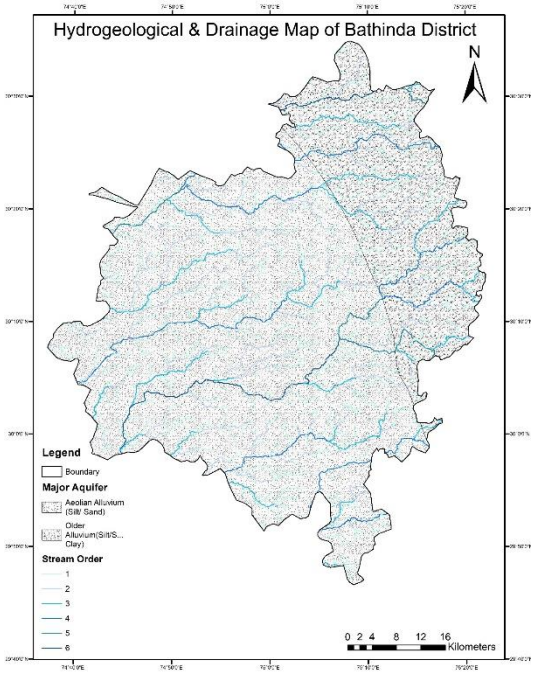

Figure 22: Hydrogeological and Drainage map of Bathinda District (Source- Bhukosh)

5.2 Groundwater Flow: Conceptual Model

A conceptual model of the study area is developed based on the hydrogeological information and field investigation. The lithologic investigation indicates that an unconfined aquifer exists in the study area. Data on study area boundary, ground and top layer, thickness of the aquifer, aquifer parameters such as hydraulic conductivity, porosity, storativity, transmissivity, specific storage, specific yield, aquifer top and bottom elevation etc. were used to develop conceptual model. The conceptual model of the study area has provided a basis for the design and development of the numerical model of the study area using USGS ModelMuse software.

Model domain and grid

To study impact of groundwater pumping on the surface and subsurface water regime a groundwater flow model was simulated, in the study area and was considered to conceptualize a groundwater model. To spatially discretize and translate the conceptual model into numerical model entire area has been discretized into columns and rows with each grid measuring 1000 m x 1000 m model.

Boundary Conditions

To account the subsurface inflows and outflows, the boundary conditions were taken as RCH (recharge package) and WEL (well package) under specified flux and EVT

(evapotranspiration package) under head dependent flux (Figure 23). The RCH includes the total inlet water in the aquifer, WEL includes the total discharge of water from the aquifer by means of wells and EVT includes the amount of evapotranspiration losses (Ansarifar et al. 2019). Precipitation data is taken from Indian Meteriological Department (https://mausam.imd.gov.in/) and evapotranspiration data from India WRIS (https://indiawris.gov.in/). The norms for rainfall infilltration factor under various hydrogeological situations are recommended in the Groundwater Resource Estimation Committee, 2009 and for Alluvial areas it is taken as 22% of average annual rainfall. The total draft in the district is given as 1333.78 mcm/ annum and the total number of pumping wells in the district is 46772. (CGWB 2017). Pumping wells are equally distributed within the district area and the discharge values of each well is calculated to be 78.13 m3/day/well i.e., 0.000904 m3/s/well.

Aquifer Properties

Table 4 shows the salient features used for groundwater modelling.

Table 4: Salient Features of the study area for Groundwater Modelling

Particulars	**Details**
District and State	Bathinda and Punjab
SOI-Toposheet Number	44J, 44K, 44N, 44O
Site Location	29° 46' 37.388" N to 30° 34' 57.527" N &
Parameter	**Value**
Grid	Grid Size: 1000 m x 1000 m
Aquifer Type	Layer 1: Unconfined/ Layer 2: Confined/ Layer 3: Confined
Boundary Conditions Used	Rainfall Recharge & evapotranspiration
Hydraulic Conductivity (K)	8.785 (m/ day)
Specific yield	7.2 %
Recharge applied	83.33 mm/year
Draft applied	1333.78 mcm/year in the district
Rainfall	381.31mm/year
Rainfall recharge (22%)	83.89 mm/year i.e., 2.66×10^{-9}
Evapotranspiration	25 mm/year i.e., 7.92745×10^{-10}

Pumping test method is the widely accepted approach to estimate the aquifer hydraulic parameters (Ansarifar et al. 2020). The hydraulic conductivity value varies from 1.6 to 19.17 m/day throughout the district and average value of 8.785 (m/ day) is considered for this study. Figure 24 shows the spatial distribution of hydraulic conductivity in the study area. The storage coefficient evaluated in the report is 2.8 x 10-2. Specific yield for the unconfined aquifer is taken as 60% of 0.12 which comes as 0.072. Aquifer-I is occurred upto a depth of 56m whereas second aquifer occurs upto a depth of 131 m and third aquifer occurs upto a depth of 300 m beneath the ground surface (CGWB 2017). Layers are generated using groundwater level observed data, which is taken from India WRIS (https://indiawris.gov.in/) and is used for cell wise interpolation through GIS software.

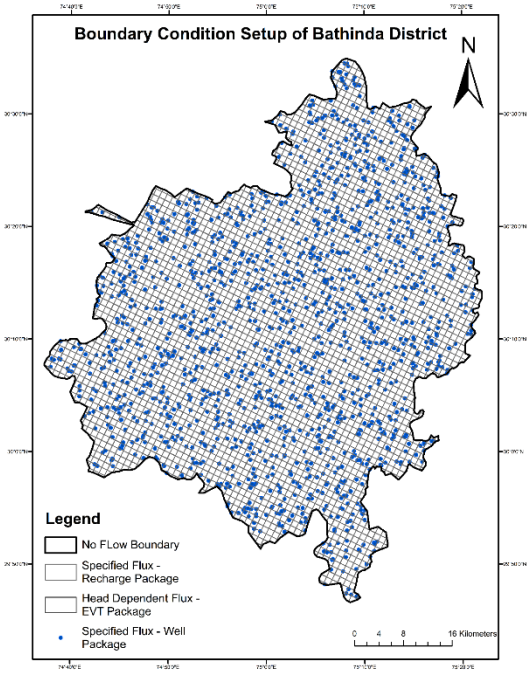
Boundary Condition Setup of Bathinda District
N
Legend
No FLow Boundary
Specified Flux - Recharge Package
Head Dependent Flux - EVT Package
Specified Flux - Well Package
0 4 8 16 Kilometers

Figure 23: Schematic diagram of Model Boundary conditions applied in the study area

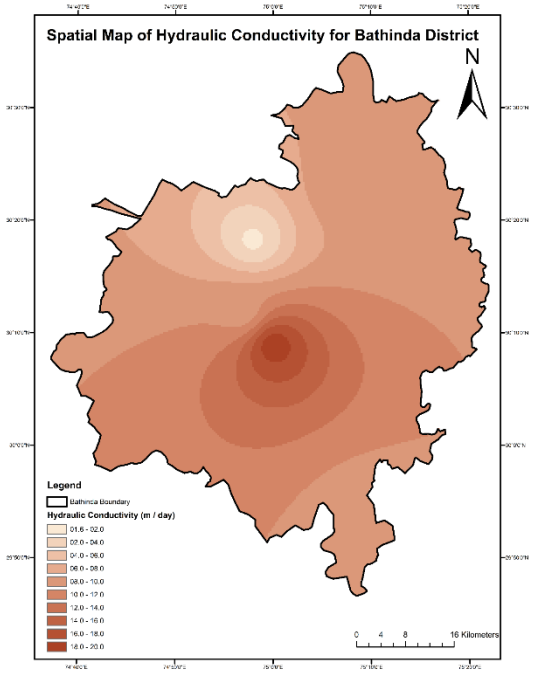

Figure 24: The spatial distribution of Hydraulic Conductivity in the study area (IndiaWRIS CGWB Well data)

Model Calibration

Based on hydrogeological and well data, Modflow model muse software has been calibrated and validated. In this simulation study, model is calibrated with the observed data from 2015 to 2020 with 365 days interval, 2015 taken as initial state of the model. Comparison of simulated (model calculated and predicted) and actual water table elevations of all eleven wells for calibration period showed that there was good match between observed and predicted water table elevation as the R^2 values were closer to

one (Figure 25). Table 5 shows the complete data of observed and calculated heads at the piezometric locations. Graphs are plotted for the observed piezometric heads and the heads calculated with the help of the model for 5 years of stress period (2015-2020). The correlation coefficient (R^2) value generated is more than 0.85 which indicates a positive correlation and sustainability of the model. The predicted head contours for the 2020 are represented in Figure 26. The groundwater heads are lying between 189.18-211.47 m amsl for 2020.

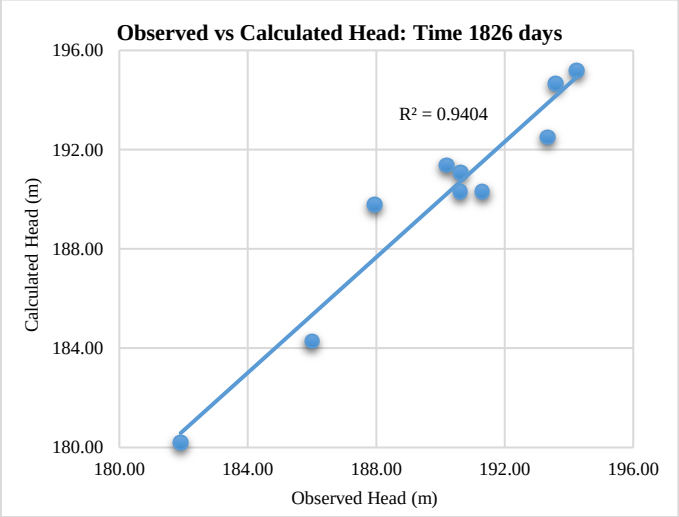

Figure 25: Observed vs Calculated Graphs for calibration from 2015 to 2020 (*Corelation coefficient, R^2= 0.9404, RMSE= 1.2311, NRMSE= 9.985%)*

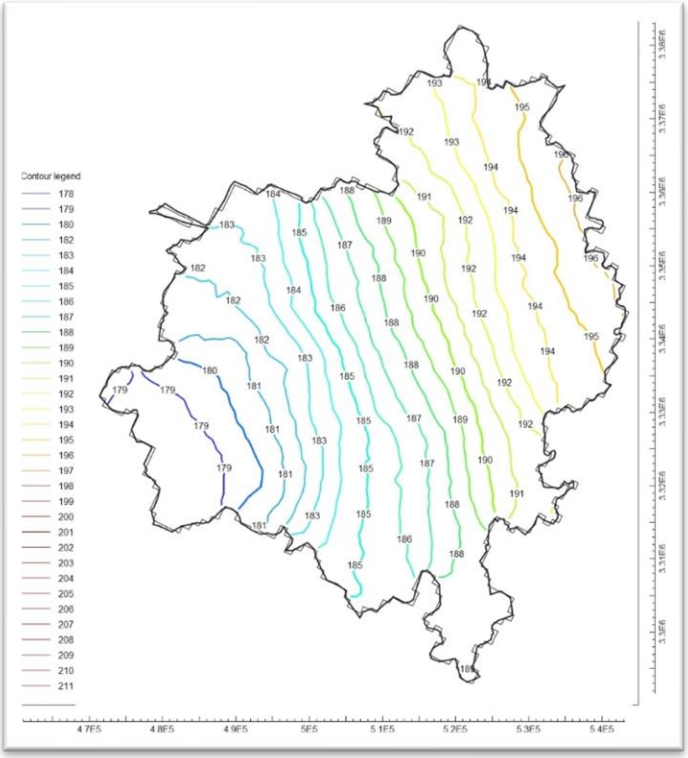

Figure 26: Contour data for heads of buffer zone of 2020

Model Prediction

After a successful calibration, we predict the scenario of groundwater availability for 2030 using the same calibrated model where it is showing that the groundwater heads are in range between 144.128-207.498 m amsl in 2030. The model outputs were received in the form of spatial variation maps of water table elevation and water budget map with their charts were generated for the different years. Table 5 shows the piezometric wells data comparison of 2030. Figure 27 shows the predicted groundwater level contour for 2030.

Table 5: Piezometric water levels in the buffer zone (calibration and prediction table)

Lat (ºE)	Long (ºN)	Village	Observed Head (m)	MODFLOW Calculated Head (m)	MODFLOW Calculated Head (m)
			2020	2020	2030
30.18	75.19	Balianwali-Pz	190.19	191.37	154.71
30.31	75.30	Bugran-Pz	193.58	194.65	157.40
30.3	74.91	Kheliwala (d)	186.00	184.27	148.16
30.26	75.20	Lehra Dhulkot-Pz	193.33	192.51	155.74
30.16	74.83	Maisar Khana-Pz	181.91	180.19	144.70
30.42	75.06	Maluka-Pz	190.63	191.06	155.52
30.31	75.08	Nathana-Pz	187.95	189.77	153.40
30.29	75.11	Phulla	191.30	190.31	153.81
30.29	75.11	Phulla1	190.61	190.31	153.81
30.36	75.30	Rayya-Pz	194.24	195.18	157.94

Groundwater Budget

The regional groundwater budget is estimated using zone budget package in Modflow. The groundwater budget for the entire study area is presented in Figure 29 which shows the volume of water in million cubic meters for different categories like storage, wells, evapotranspiration and recharge with blue color as input (recharge) of water and red as output (draft) of water from the buffer zone. The recharge volume in the graph is insufficient to fulfill the draft by the wells which means there is more extraction of water from the aquifer and it's been fulfilled by

the groundwater storage potential. Water budget for a 10-year period i.e., from 2020 to 2030 indicates a significant reduction in the groundwater storage from 986.332 to 930.286 MCM per annum as there has been an increase in groundwater abstraction from 87,040 to 243,712 m^3 per annum. The prediction of 2030 shows that the area will suffer from scarcity of groundwater as it is already an Over Exploited Category (CGWB, Block wise Ground Water Resource Assessment, 2020). The mass balance output table from MODFLOW for 2030 is given in Figure 30 which shows the values generated from modelling in the year 2030 i.e., 15th stress period.

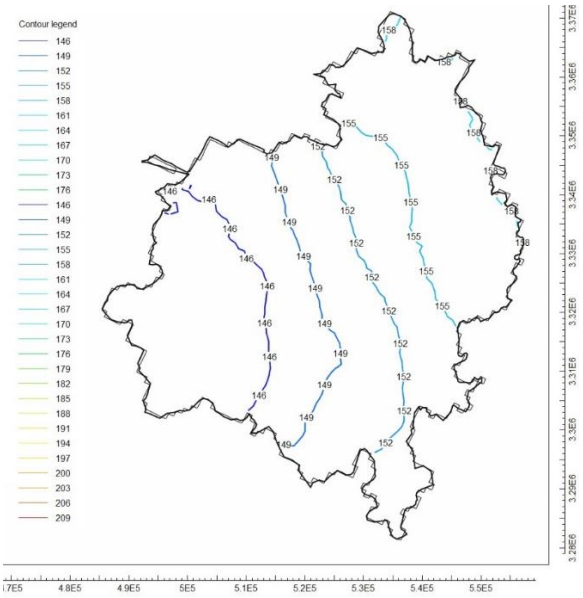

Figure 27: Contours of predicted head of the year 2030

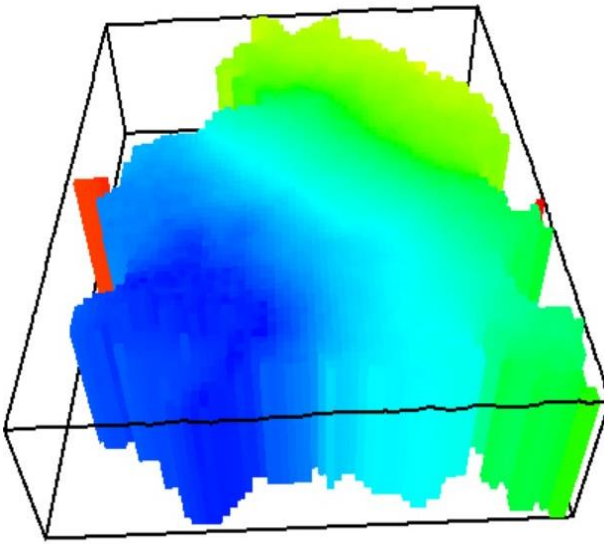

Figure 28: 3D view of 2030

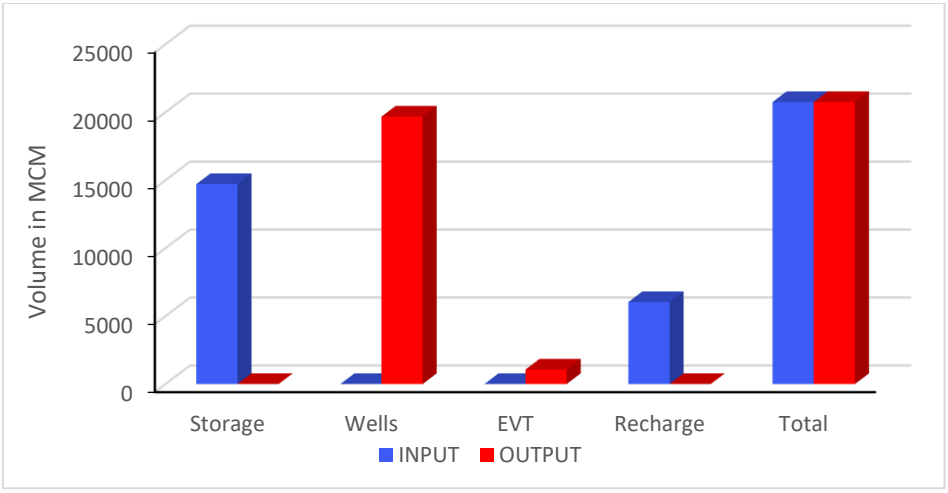

Figure 29: graph showing the calculated mass balance of the year 2030

```
 VOLUMETRIC BUDGET FOR ENTIRE MODEL AT END OF TIME STEP    1, STRESS PERIOD  15
 ------------------------------------------------------------------------------

    CUMULATIVE VOLUMES      L**3       RATES FOR THIS TIME STEP      L**3/T
    ------------------                 ------------------------

          IN:                                   IN:
          ---                                   ---
            STORAGE = 14714448896.0000            STORAGE =          29.4992
      CONSTANT HEAD =           0.0000      CONSTANT HEAD =           0.0000
              WELLS =     1826238.2500              WELLS =           0.0000
           RECHARGE =  6036236288.0000           RECHARGE =          12.3120
         ET SEGMENTS =           0.0000         ET SEGMENTS =           0.0000

            TOTAL IN = 20752510976.0000            TOTAL IN =          41.8112

          OUT:                                  OUT:
          ----                                  ----
            STORAGE =      185098.2031            STORAGE =           0.0000
      CONSTANT HEAD =           0.0000      CONSTANT HEAD =           0.0000
              WELLS = 19682400256.0000              WELLS =          39.9649
           RECHARGE =           0.0000           RECHARGE =           0.0000
         ET SEGMENTS =  1070170304.0000         ET SEGMENTS =           1.8466

           TOTAL OUT = 20752754688.0000           TOTAL OUT =          41.8115

            IN - OUT =     -243712.0000            IN - OUT =      -2.7466E-04

 PERCENT DISCREPANCY =          -0.00     PERCENT DISCREPANCY =          -0.00
```

Figure 30: Mass balance output from MODFLOW 2030

5.3 Sensitivity analysis

It is seen that the results of the presented simulation model is in agreement with the observed solution. However, to make the model stable and converge fast one needs to see the parameters with which the model is sensitive to. For the groundwater flow, if hydrogeological parameters like hydraulic conductivity and storativity are kept constant, then there are three parameters on which the model depends on. These are the inter-nodal distance (ΔX, ΔY) and time interval (Δt).

Sensitivity of inter-nodal distance (*ΔX, ΔY*)

To see the sensitivity of the model with respect to inter-nodal distance it is run for ΔX, ΔY = 500m, 1000m, 1500m and Δt = 365days. The % error between the model result and the observed solution is minimum for ΔX, ΔY = 1000m. Figure 31 gives the comparison of % error for Spatial variation.

Sensitivity of time step (*Δt*)

To see the sensitivity of the model with respect to time step it is run for Δt = 182 days, Δt = 365 days, Δt = 3652 days with ΔX, ΔY = 1000m. It is found that the % error between model result and analytical solution is minimum for Δt = 365 days. Figure 32 gives the comparison of % error for temporal variation.

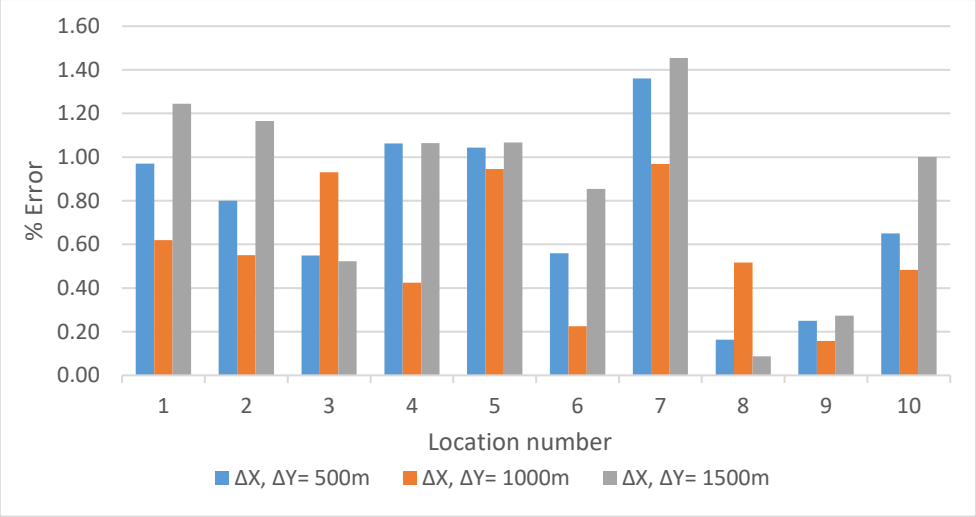

Figure 31: Sensitivity of inter-nodal distance (ΔX, ΔY)

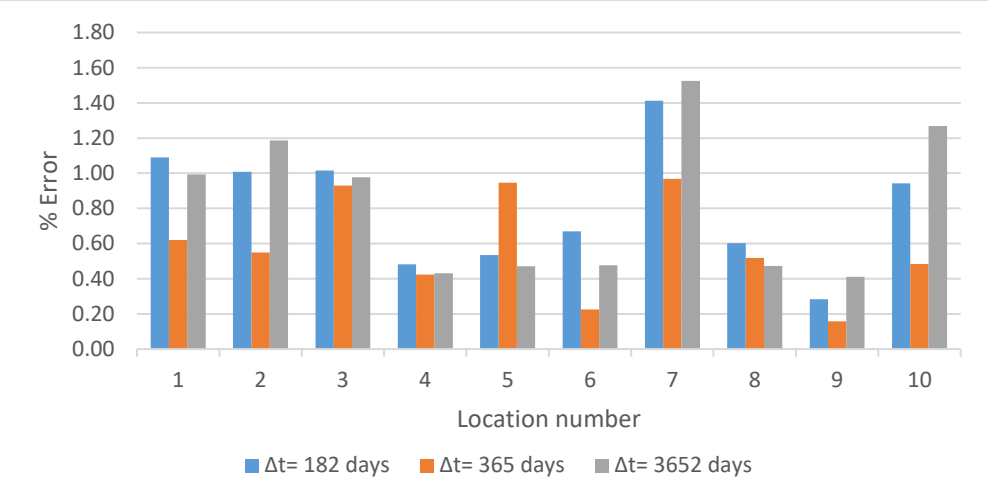

Figure 32: Sensitivity of temporal variation

5.4 Uranium Transport: Conceptual Model

The groundwater flow model is now taken to the next stage i.e., MT3DMS for contaminant transport for Uranium as contaminant. The Initial uranium concentration is taken as zero and uranium transport model is run for a longitudinal dispersity of 160 (Bhosale et.al. 2001) and mass loading was input by trail method as per Table 6 using sink and source mixing package.

Model Calibration

In this simulation study, MT3D results is calibrated using the observed data of the year 2020 taken from CGWB, 2020. The model is run from 2015 to 2020 with 365 days interval, taking 2015 as initial state. Comparison of simulated and observed uranium content as per CGWB-June 2020, 'Uranium Occurrence in Shallow Aquifers in India' for calibration period showed that there was good match between observed and calculated uranium contamination as the R^2

values were closer to one i.e., 0.9962. Table 6 shows the complete data of observed and calculated uranium concentration eight locations. Graphs are plotted for the observed concentration and the concentration calculated with the help of the model for 5 years of stress period (2015-2020). The correlation coefficient (R^2) value generated is more than 0.85 which indicates a positive correlation and sustainability of the model (Figure 33). The calculated uranium concentration lies between 19.55-82.314 ppb for 2020. Figure 34 shows the plume contour of uranium concentration in Bathinda district using data from CGWB report- June 2020, Uranium Occurrence in Shallow Aquifers in India.

Model Prediction

After a successful calibration, we predict the scenario of Uranium concentration for 2030 using the same calibrated model, where it is showing that the Uranium concentration are in range between 9.21-147.72 ppb in 2030. The model outputs were received in the tabular form and contour map was made using Arc GIS as shown in Figure 34. Table 6 shows the Uranium concentration data comparison of 2020 and 2030.

Table 6: Uranium concentration in the buffer zone (calibration and prediction table)

Lat (ºE)	Long (ºN)	Village	Observed U concentration (ppb)	MODFLOW Calculated U concentration (ppb)	MODFLOW Calculated U concentration (ppb)
			2020	2020	2030
30°13'24"	74°46'59"	Balluana	44.5	46.02	75.09
30°20'14"	74° 47'19"	Ablu	68	69.09	117.97
30°18'29"	74°54'31"	Nahian wala	71	70.88	116.79
30°15'17"	74°56'02"	Dera tappa	82.5	82.31	147.73
30°16'04"	75°14'35"	Rampur-phul	42.9	42.62	72.25
30°14'07"	75°19'13"	Badiala	41.5	40.75	70.33
30°07'46"	74°40'17"	Raike kalan	31.4	34.06	54.18
30°07'30"	74°47'31"	Ghudda	33.1	35.65	58.17

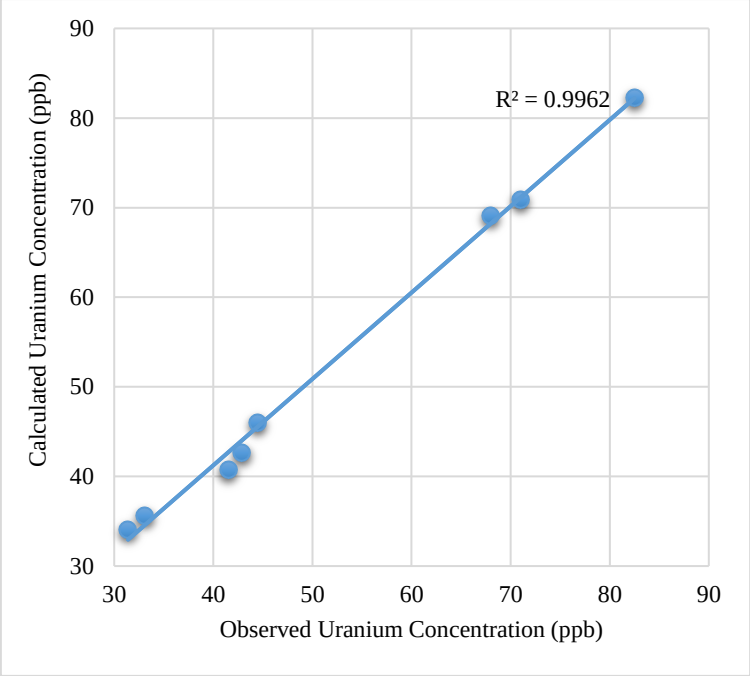

Figure 33: Observed vs Calculated Graphs for calibration of uranium concentration from 2016 to 2021 (*Corelation coefficient, R^2= 0.9962, RMSE= 1.4894, NRMSE= 2.90%)*

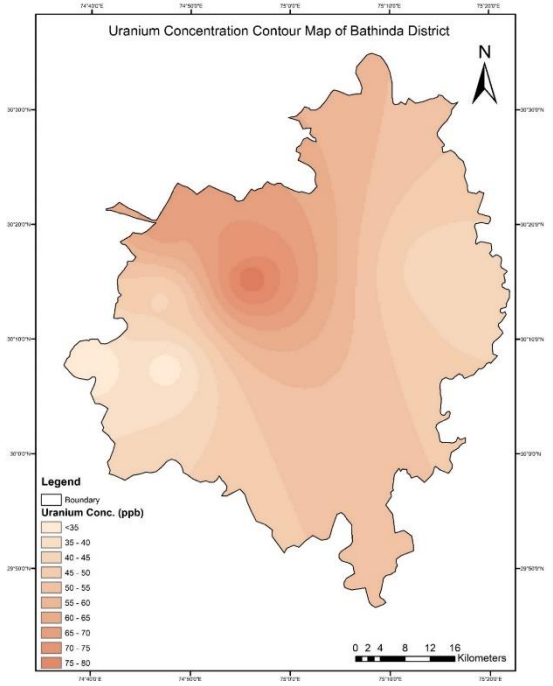

Figure 34: Uranium concentration contour map of Bathinda District for the year 2020 (CGWB-June 2020).

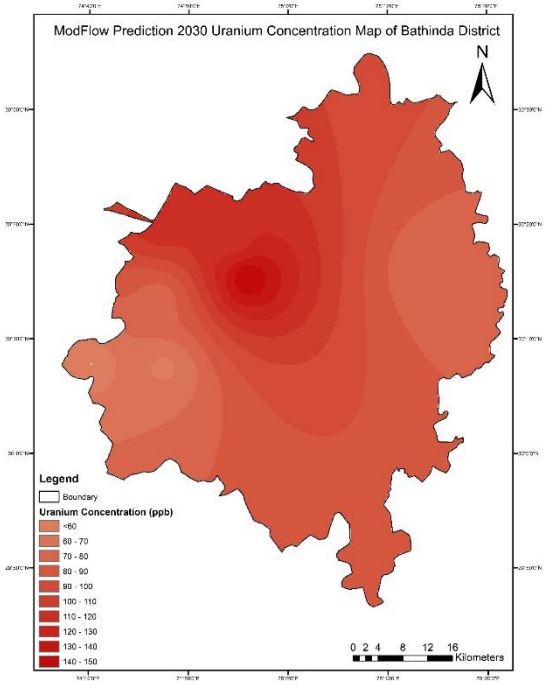

Figure 35: Uranium concentration contour map of Bathinda District for the year 2030.

5.5 Lead Transport: Conceptual Model

The groundwater flow model was again set up for 2008 as the initial time and 2013 as the calibration time using the initial head as the head for the year 2008 as per CGWB exploration

wells. This model was well calibrated with R^2=0.8778, RMSE= 3.054m and NRMSE= 34%. After a successful calibration the flow model is now taken to the next stage i.e., MT3DMS for contaminant transport for Lead as contaminant. The Initial Lead concentration is taken as 10 and transport model is run for a longitudinal dispersity of 160 (Bhosale et.al. 2001) and mass loading was input by trail method as per Table 7 using sink and source mixing package.

Model Calibration

In this simulation study, MT3D results is calibrated using the observed data of the year 2020 taken from Tajinder Kaur et. al., 2021. The model is run from 2008 to 2013 with 365 days interval, taking 2008 as initial state. Comparison of simulated and observed lead content as per Tajinder Kaur et. al., 2021 demonstrated that the observed and calculated values for the calibration period were well-matched as the R^2 values were closer to one i.e., 0.9962 (Figure 36). Table 7 shows the complete data of observed and calculated lead concentration nine locations.

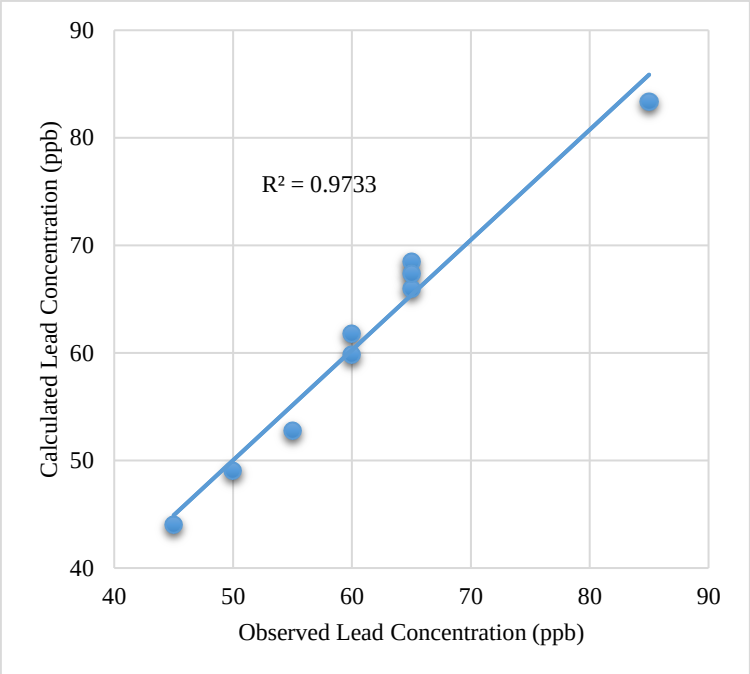

Figure 36: Observed vs Calculated Graphs for calibration of lead concentration from 2016 to 2021 (*Corelation coefficient, R^2= 0.9992, RMSE= 1.767, NRMSE= 17.60%)*

Model Prediction

After a successful calibration, we predict the scenario of lead concentration for 2030 using the same calibrated model, where it is showing that the lead concentration are in range between 64.55- 618.51 ppb in 2030. The model outputs were received in the tabular form and contour map was made using Arc GIS as shown in Figure 35. Table 7 shows the lead concentration data comparison of 2013 and 2030.

Table 7: Lead concentration in the buffer zone (Observed and prediction table)

Latitude (ºE)	Longitude (ºN)	Location no.	Observed Pb concentration (ppb)	MODFLOW Calculated Pb concentration (ppb)
			2013	2030
30.063592	74.773325	GWS 9	50	64.55
30.212399	74.784158	GWS 10	60	86.38
30.016876	74.949983	GWS 11	65	108.21
30.002328	75.020600	GWS 12	65	121.79
30.267533	75.089592	GWS 14	65	111.14
30.450265	75.108424	GWS 15	55	98.60
30.477703	75.160734	GWS 16	45	60.68
30.304496	75.262962	GWS 17	60	96.27
30.121880	75.184340	GWS 18	85	143.87
30.259474	74.968490	GWS 13	285	618.51

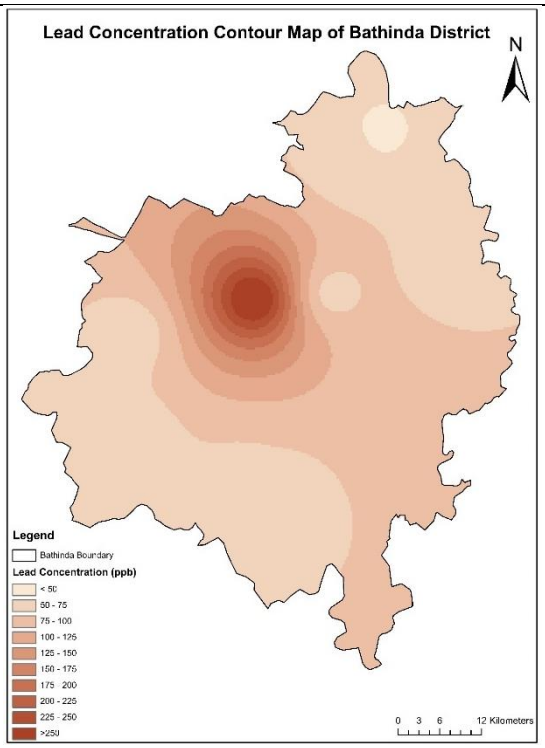

Figure 34: Lead concentration contour map of Bathinda District for the year 2020 (Tajinder Kaur et. al., 2021).

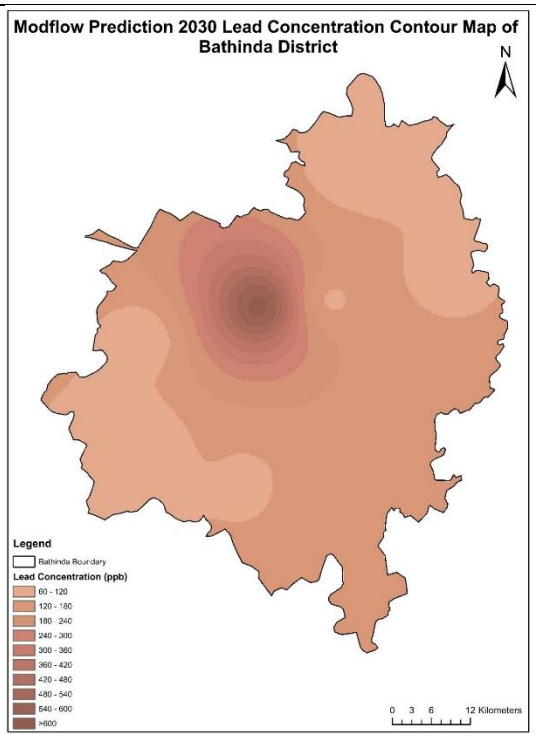

Figure 35: Lead concentration contour map of Bathinda District for the year 2030.

5.6 Conclusion

In this study, groundwater modelling is carried out for Bhatinda, Punjab, India using MODFLOW and MT3D. The model results indicate that if the depletion in the groundwater will sustain, the area will fall under the groundwater deficit zone at the end of year 2030. It is observed that the undue exploitation of groundwater has adversely affected the availability and quality of groundwater in Bathinda District. The southwestern part of the study area will dry up first as compared to the other parts. The Uranium concentration is predicted to reach up to a maximum value of 147.72 ppb and lead concentration can reach upto a maximum value of 618.51 ppb within the district which implies that the groundwaters of Bathinda District shall not be safe for drinking in future. MODFLOW can be efficiently implemented to the confined/unconfined aquifers with the consideration of aquifer characteristics and boundary conditions. It makes the flow and transport simulation feasible for vast areas and large number of grids. It acts as a tool in predicting the future scenarios, which aids in taking appropriate preventive measures to ensure the availability of acceptable quality of potable water in the times to come.

6. Future Scope and Limitations

Contribution 1: Biosorption of lead II using Foeniculum Vulgare in the aqueous phase

Future Scope

- The future scope of this study is to investigate and identify the efficiency of the fennel biosorbent for removal of different heavy metals.
- Another future scope is to identify different new biosorbents for removal of heavy metals from the aqueous solution.

Limitations

The study has the limitations of synthetic sample being used for the experimentation. In case of real sample, the efficiency of lead removal will vary depending on the concentration and interference of other heavy metals in the solution.

Contribution 2: Case Study- MODFLOW/ MT3D groundwater flow and Uranium and Lead Transport of Bathinda district, Punjab, India

Future Scope

- The future scope of this study is to investigate and identify the source and actual cause of higher uranium and lead concentrations.

- Another future scope can be identifying other major contaminants in the groundwater and predict its flow and transport to get a better picture of the situation in the near future.
- The model can be extended for remediation of uranium/ Lead and prediction of the remediation plume.
- This model can be used to identify the uranium/ lead transport in other parts of the world.

Limitations

The study has the limitations of unavailability of town wise uranium/ lead concentration data and lack of information on proper cause of uranium contamination in the groundwaters of the Bathinda district, India.

The experimentation of uranium was not allowed and therefore remediation couldn't be performed.

7. Publications

✓ **Paper Published**

"Biosorption of lead II using Foeniculum Vulgare in the Aqueous Phase" published in ***Journal of Hazardous Toxic and Radioactive Waste*** © ASCE, ISSN 2153-5493- DOI: 10.1061/(ASCE)HZ.2153-5515.0000709

✓ **Paper Published**

"MODFLOW/ MT3D based three-dimensional groundwater flow and transport simulation of Uranium contamination in Bathinda District of Punjab, India" is accepted in ***Journal of Hazardous Toxic and Radioactive Waste*** © ASCE, ISSN 2153-5493

✓ **Paper in progress**

"Groundwater flow and transport using Meshfree collocation method with Cubic Spline Function" communicated to ***Modelling Earth Systems and Environment by Springer.***

✓ **Paper presented (Conference)**

A paper titled "Remediation Techniques for Groundwater Contaminated With Radionuclide", Was presented during 22nd International Conference on Hydraulics, Water Resources & Coastal Engineering. ***HYDRO-2017***, held at L.D. college of engineering, Ahmedabad during 21-23 December, 2017.

✓ **Workshop attended**

Attended a 10 days' workshop of Global Initiative of Academic Networks (GIAN) on "Transport of Viruses and Colloids in subsurface soil and groundwater" at Department of Hydrology, ***IIT Roorkee***, 12-20 February 2019.

8. References

- Ansarifar MM., Salarijazi M., Ghorbani K. & Kaboli AR. (2019). Simulation of groundwater level in a coastal aquifer. Marine Georesources & Geotechnology. 38. 1-9. https://doi.org/10.1080/1064119X.2019.1639226
- Ansarifar MM., Salarijazi M., Ghorbani K. & Kaboli AR. (2020). Spatial estimation of aquifer's hydraulic parameters by a combination of borehole data and inverse solution. Bull Eng Geol Environ 79, 729–738. https://doi.org/10.1007/s10064-019-01616-w
- Bhosale D. and Kumar C.P. (2002). Simulation of Seawater Intrusion in Ernakulam Coast. International Conference on "Hydrology and Watershed Management", 18-20 December 2002.
- B.S. Bajwa, Sanjeev Kumar, Surinder Singh, S.K. Sahoo, R.M. Tripathi, Uranium and other heavy toxic elements distribution in the drinking water samples of SW-Punjab, India, Journal of Radiation Research and Applied Sciences, Volume 10, Issue 1, 2017, Pages 13-19. DOI: 10.1016/j.jrras.2015.01.002
- CGWB (2017). Aquifer Mapping and Management Plan Bhatinda District, Punjab. Government Of India. Ministry of Water Resources, River Development and Ganga Rejuvenation. Central Ground Water Board. Retrieved from: http://cgwb.gov.in/AQM/NAQUIM_REPORT/Punjab/Bhatinda.pdf
- CGWB (2020). Uranium occurrence in shallow aquifers in india. Government Of India. Ministry of Water Resources, River Development and Ganga Rejuvenation. Central Ground Water Board. Retrieved from: http://cgwb.gov.in/WQ/URANIUM_REPORT_2019-20.pdf
- CGWB, Block wise Ground Water Resource Assessment. (2020). Government Of India. Ministry of Water Resources, River Development and Ganga Rejuvenation. Central Ground Water Board. Retrieved from: http://cgwb.gov.in/GW-Assessment/2021-08-02-GWRA-2020-BLOCKWISE%20MASTERSHEET.pdf
- D. Ringot, B. Lerzy, K. Chaplain, J.-P. Bonhoure, E. Auclair, and Y. Larondelle (2007) In vitro biosorption of ochratoxin A on the yeast industry by-products: comparison of isotherm models. Bioresource Technology, vol. 98, no. 9, pp. 1812–1821.
- Ebelegi, Augustus & Nimibofa, Ayawei & Donbebe, Wankasi. (2020). Interpretation of Adsorption Thermodynamics and Kinetics. Open Journal of Physical Chemistry. 10. 166-182. 10.4236/ojpc.2020.103010.

- H. Shahbeig, N. Bagheri, S. A. Ghorbanian, A. Hallajisani, and S. Poorkarimi (2013) A new adsorption isotherm model of aqueous solutions on granular activated carbon. World Journal of Modelling and Simulation, vol. 9, no. 4, pp. 243–254.
- Hosseini-Bandegharaei, M. S. Hosseini, M. Sarw-Ghadi, S. Zowghi, E. Hosseini, H. Hosseini-Bandegharaei (2010) Kinetics, equilibrium and thermodynamic study of Cr(VI) sorption into toluidine blue o-impregnated XAD-7 resin beads and its application for the treatment of wastewaters containing Cr(VI). Chemical Engineering Journal 160, 190–198.
- Jaspal Singh, Lakhwant Singh, Surinder Singh, High U-contents observed in some drinking waters of Punjab, India, Journal of Environmental Radioactivity,Volume 26, Issue 3, 1995, Pages 217-222, DOI: 10.1016/0265-931X(94)00037-W
- J. N. Ghogomu1, T. D. Noufame, M. J. Ketcha and N. J. Ndi (2013) Removal of Pb(II) Ions from Aqueous Solutions by Kaolinite and Metakaolinite Materials. British Journal of Applied Science & Technology 3(4): 942-961.
- J. S. Piccin, G. L. Dotto and L. A. A. Pinto (2011) Adsorption isotherms and thermochemical data of FD&C RED N° 40 binding by chitosan. Brazilian Journal of Chemical Engineering Vol. 28, No. 02, pp. 295 – 304.
- Liangshu Xia et al. (2013), Uranium Removal from Aqueous Solution by Banyan Leaves: Equilibrium, Thermodynamic, Kinetic, and Mechanism Studies. American Society of Civil Engineers. Vol. 139, No. 6:887-895.
- Liu, G.R. (2003). Mesh Free Methods: Moving beyond the Finite Element Method. CRC Press, Boca Raton, USA.
- M. Temkin, V. Pyzhev (1940) Recent modifications to Langmuir isotherms, Acta Physicochim. USSR 12, 217–222.
- Muhammad Tahir Amin, Abdulrahman Ali Alazba and Muhammad Shafiq (2015) Adsorptive Removal of Reactive Black 5 from Wastewater Using Bentonite Clay: Isotherms, Kinetics and Thermodynamics. Sustainability 2015, 7, 15302-15318.
- Robert Brooks et al. (2010), Removal of lead from contaminated water. International Journal of Soil, Sediment and Water, Volume 3 Issue 2 Article 14.
- S. Y. Lagergren, Zur Theorie der sogenannten Adsorption geloster Stoffe, Kungliga Svenska Vetenskapsakad (1898). Handlingar 24, 1–39.

- Sana Solat et al. (2014) Biosorption of Uranium from Aqueous Solution by Live and Dead Aspergillus niger. (ASCE)HZ.2153-5515.
- Sushant Kumar, M. K. Choudhary, T. R. Nayak. (2017). Groundwater Modelling in Bina River Basin, India using Visual. IJSRD - International Journal for Scientific Research & Development Vol. 5, Issue 05.
- Tajinder K., Sneh R., Renu B., Priyanka B. & Saroj A. (2021). Appraisal of heavy metal pollution in groundwater of Malwa region, Punjab (India) using stress biomarkers in Brassica juncea. Environmental Earth Sciences. 80. 362. DOI: 10.1007/s12665-021-09657-9.
- Venkateswara Rao Surisetty, Janusz Kozinski, and L.Rao Nageswara (2013) Biosorption of Lead Ions From Aqueous Solution Using Ficus benghalensis L. Journal of Engineering Vol 2013 Article ID-167518.
- Zaynab Aly, Adrien Graulet, Nicholas Scales and Tracey Hanley (2014) Removal of aluminium from aqueous solutions using PAN-based adsorbents: characterisation, kinetics, equilibrium and thermodynamic studies. Environmental Science and Pollution Research 21:3972–3986.